ACTA UNIVERSITATIS LODZIENSIS
Folia Geographica Physica 19, 2020: 7–18, https://doi.org/10.18778/1427-9711.19.01
KATEDRA GEOGRAFII FIZYCZNEJ
Uniwersytet Łódzki

Polina Lemenkova

Schmidt Institute of Physics of the Earth of the Russian Academy of Sciences, Department of Natural Disasters, Anthropogenic Hazards and Seismicity of the Earth, Laboratory of Regional Geophysics and Natural Disasters
E-mail: *pauline.lemenkova@gmail.com*

GEBCO and ETOPO1 gridded datasets for GMT based cartographic Mapping of Hikurangi, Puysegur and Hjort Trenches, New Zealand

Rastrowe zestawy danych GEBCO i ETOPO1 dla kartowania opartego na GMT Kartowanie rowów Hikurangi, Puysegur i Hjort, Nowa Zelandia

Abstract The study focused on the comparative analysis of the submarine geomorphology of three oceanic trenches: Hikurangi Trench (HkT), Puysegur Trench (PT) and Hjort Trench (HjT), New Zealand region, Pacific Ocean. HjT is characterized by an oblique subduction zone. Unique regional tectonic setting consist in two subduction zones: northern (Hikurangi margin) and southern (Puysegur margin), connected by oblique continental collision along the Alpine Fault, South Island. This cause variations in the geomorphic structure of the trenches. PT/HjT subduction is highly oblique (dextral) and directed southwards. Hikurangi subduction is directed northwestwards. South Island is caught in between by the "subduction scissor". Methodology is based on GMT (The Generic Mapping Tools) for mapping, plotting and modelling. Mapping includes visualized geophysical, tectonic and geological settings of the trenches, based on sequential use of GMT modules. Data include GEBCO, ETOPO1, EGM96. Comparative histogram equalization of topographic grids (equalized, normalized, quadratic) was done by module 'grdhisteq', automated cross-sectioning – by 'grdtrack'.

Results shown that HjT has a symmetric shape form with comparative gradients on both western and eastern slopes. HkT has a trough-like flat wide bottom, steeper gradient slope on the North Island flank. PT has an asymmetric V-form with steep gradient on the eastern slopes and gentler western slope corresponding to the relatively gentle slope of a subducting plate and steeper slope of an upper one. HkT has shallower depths < 2,500 m, PT is <-6,000 m. The deepest values > 6,000 m for HjT. The surrounding relief of the HjT presents the most uneven terrain with gentle slope oceanward, and a steep slope on the eastern flank for PT, surrounded by complex submarine relief along the Macquarie Arc. Data distribution for the HkT demonstrates almost equal pattern for the depths from -600 m to -2,600 m. PT has a bimodal data distribution with 2 peaks: 1) -4,250 to -4,500 m (18%); 2) -2,250 to -3,000 m, < 7,5%. The second peak corresponds to the Macquarie Arc. Data distribution for HjT is classic bell-shaped with a clear peak at -3,250 to -3,500 m. The asymmetry of the trenches resulted in geomorphic shape of HkT, PT and HjT affected by geologic processes.

Keywords GMT, Hikurangi Trench, Puysegur Trench, Hjort Trench, geomorphic modelling, cartography, visualization, data analysis, bathymetry, Pacific Ocean.

Zarys treści Studium poświęcone jest analizie porównawczej rzeźby dna trzech rowów oceanicznych: Hikurangi (HkT), Puysegur (PT) i Hjort (HjT), położonych w pobliżu Nowej Zelandii na południowym Pacyfiku. HjT charakteryzuje się skośną strefą subdukcji. Unikalna sytuacja geotektoniczna regionu polega na rozdzieleniu dwóch stref subdukcji: północnej (Hikurangi) i południowej (Puysegur), strefą kolizji kontynentalnej wzdłuż uskoku Alpine Fault na Wyspie Południowej. Subdukcja na południe od Wyspy Południowej zachodzi pod dużym kątem w kierunku południowo-wschodnim (PT i HjT), podczas gdy w strefie północnej (Hikurangi) odbywa się na północny zachód. W konsekwencji Wyspa Południowa jest ujęta w swego rodzaju „nożyce subdukcyjne". Metodologia oparta na GMT (The Generic Mapping Tools) posłużyła do skartowania, wykreślenia i modelowania obszaru. Kartowanie obejmuje wizualizację danych geofizycznych oraz pozycji tektonicznej i geologicznej rowów, opartą na sekwencyjnym użyciu modułów GMT. Dane obejmują GEBCO, ETOPO1, EGM96. Porównawcza korekcja histogramu siatek topograficznych (wyrównana, znormalizowana, kwadratowa) została wykonana przez moduł „grdhisteq", zaś zautomatyzowane przekroje – przez moduł „grdtrack".

Analiza wykazała , że rów Hjort ma symetryczną formę z porównywalnymi nachyleniami zarówno na zachodnich, jak i wschodnich zboczach. Rów Hikurangi ma podobne do koryta płaskie szerokie dno, a stok od strony zachodniej (przylegający do Wyspy Północnej) jest nachylony pod większym kątem od stoku wschodniego. Rów Puysegur ma asymetryczną V-kształtną formę ze stromo nachylonym zboczem wschodnim i łagodniejszym zachodnim. Rów HkT jest relatywnie płytki < 2500 m, PT osiąga głębokość <-6000 m. Największą głębokość (> 6000 m) stwierdzono dla rowu Hjort. Rzeźba dna w otoczeniu HjT jest najbardziej zróżnicowana, a w przypadku położonego bardziej na północ PT zaznacza się wyraźna dysproporcja pomiędzy łagodnym oceanicznym zboczem na zachodzie i stromym zboczem grzbietu Puysegur (północny odcinek Łuku Macquarie) na wschodniej flance rowu. Rozkład danych batymetrycznych dla HkT jest stosunkowo zrównoważony dla głębokości od 600 m do 2600 m. PT ma bimodalny rozkład danych z 2 pikami: 1) 4250 do 4500 m (18%); 2) 2250 do 3000 m, < 7,5%. Druga koncentracja danych odpowiada łukowi Macquarie. Rozkład danych dla HjT ma klasyczny kształt dzwonu z wyraźnym ekstremum odpowiadającym głębokościom 3250 do 3500 m. Asymetria zaprezentowanych rowów oceanicznych jest uwarunkowana przez procesy geotektoniczne.

Słowa kluczowe GMT, rów Hikurangi, rów Puysegur, rów Hjort, modelowanie geomorfologiczne, kartografia, wizualizacja, analiza danych, batymetria, Ocean Spokojny.

1. Introduction

Worldwide, deep-sea ocean trenches are mostly formed in the locations of the subduction zones of plate, along which lithospheric tectonic plates subduct one under another. Morphologically presented as long, narrow, steep-sided depressions in the ocean bottom, hadal trenches typically occur in the maximum oceanic depths, ca 7,300 up to >11,000 m (e.g. Mariana Trench). The geomorphic appearance of hadal trenches is their cross-sections is highly variable (V-shaped, U-shaped, elongated to upside-down-ridge-like, circular-like, arcuate, symmetric of irregular: left- or right-sided), which is often related to the prevailing tectonic plate movements, geologic regime and substrate, contributing to the geomorphic shape of the trenches.

The focus of this study is set on the comparative analysis of the three oceanic trenches: Hikurangi, Puysegur and Hjort, located near New Zealand, southwest Pacific Ocean (Fig. 1). Unique tectonic setting of the region consist in the connection of two subduction zones in the north (Hikurangi margin) and in the south (Puysegur margin), connected by an oblique continental collision along the Alpine Fault located in the South Island of New Zealand. This cause variations in the submarine geomorphic structure of the trenches which is also referred as "subduction scissor" (Pysklywec *et al*. 2010).

The Puysegur/Hjort subduction is highly oblique (dextral) and directed southeastwards. The Hikurangi subduction is directed northwestwards. Hence, the South Island is caught in between by the "subduction scissor". In the absence of available high-resolution information and detailed mapping on the seabed geomorphology of the Hikurangi, Puysegur and Hjort trenches, a GMT approach to map their seafloor on a local scale were undertaken. Since seafloor of the deep-sea trench represents an integrated response to a complex range of factors, such as oceanographic, geological and tectonic conditions which eventually define the present shape of the seabed landforms, an integrated approach was used to visualize, model and map three trenches on the New Zealand margin.

In this study, following key questions were addressed: the most repetitive depths of the seafloor of the trenches, and analysis of variations in the trench geomorphology. The cross-section modelling was performed via GMT modules ‚psxy' and ‚grdtrack'.

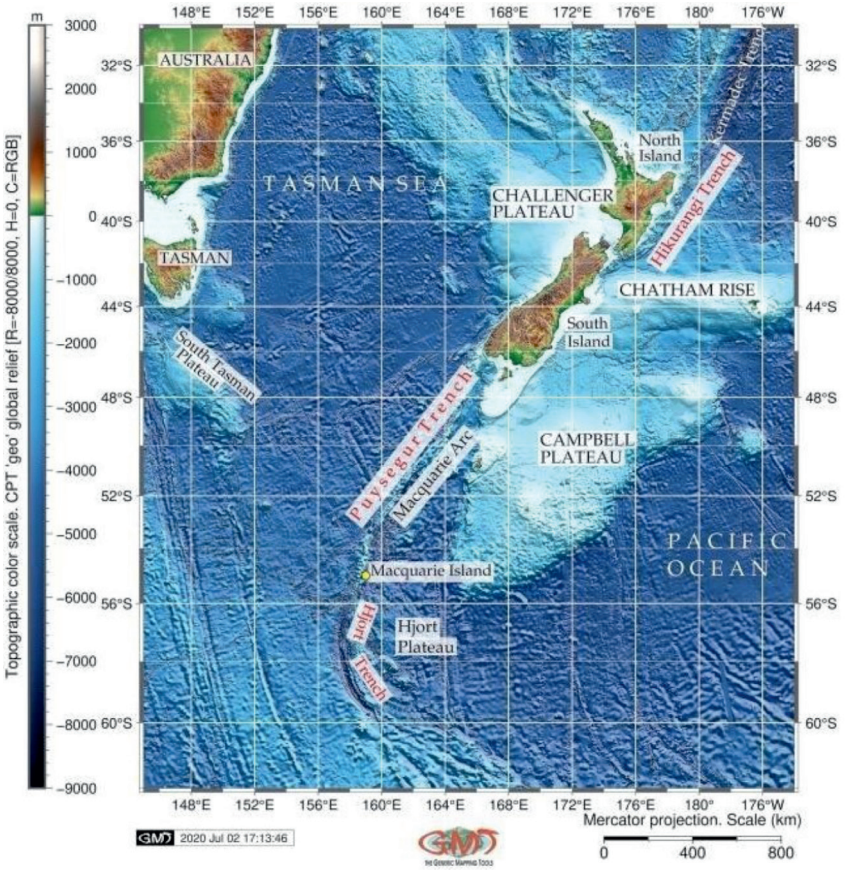

Fig. 1. GEBCO based topographic map of the New Zealand, Hikurangi, Puysegur and Hjort Trenches (ed. by author)

Ryc. 1. Mapa topograficzna Nowej Zelandii i rowów oceanicznych Hikurangi, Puysegur i Hjort w oparciu o GEBCO (oprac. autorki)

2. Study area

2.1. Hikurangi Trench

The Hikurangi Trench (sometimes also referred as trough) is located on the Hikurangi margin which is 500 km long by 480 km wide (Nicol, Wallace 2007), located northeast from the North Island. The toponymy of the Hikurangi Trench vary in the existing literature due to its specific geomorphology: in some works it is referred as 'trench' (e.g. Reyes *et al*. 2010; Reyners *et al*. 2011; Clark *et al*. 2019), in other works – as 'trough' (e.g. Barnes *et al*. 2010; Greinert *et al*. 2010; Jiao *et al*. 2015; Jiao *et al*. 2017).

The tectonic location of the Hikurangi is at the southern end of the 1000 km long Tonga-Kermadec--Hikurangi subduction systems, where Pacific Plate subducts obliquely northwestwards beneath the Indo--Australian Plate (Barnes, Mercier de Lepinay 1997) and Indo-Australian Plate has a strike-slip motion at 4 cm/yr. Comparing to the Kermadec trench reaching up to 9000 m, Hikurangi trench is shallow (ca. 3000 m). Pacific Plate dips at Hikurangi trench at a gentle angle of about 3° for at least 100 km beneath the trench and then further steepens beneath the North Island (Barker *et al*. 2009). The Alpine Fault stretches sub-parallel to the western edge of the Hikurangi Trench (Fig. 2). The speed of subduction on the Hikurangi Margin varies with a general trend of increase northwards: 34 mm/yr in the south (westward off Bounty Trough), 38 mm/yr in its central part (North Island) and 47 mm/yr in the North Island (Reyners 2013).

The Hikurangi north-west dipping subduction zone is old (started ca. 20 Ma). The subducted slab has a well defined Wadati-Benioff zone and steepens from shallow angles near the surface to near-vertical at depths > 100 km (Ballance 1976).

The geophysical, topographic and geological settings of the Hikurangi margin vary along the trench from south to north (Wallace *et al*. 2009), comparing Figure 2, 3, 4 and 5. Thus, interseismic coupling is strong and deep in the south, then gradually shallows northwards and becomes shallow and weak in the north. Southern region is characterized by accretionary wedge and tectonic contraction in the forearc. Northern region is characterized by frontal subduction erosion, numerous seamounts, and a slightly extensional upper plate. Kinematics of the Hikurangi Margin studied by GPS measurements of the horizontal velocity fields (Nicol, Wallace 2007) shown changes in faulting along the margin and clockwise tectonic block rotations caused by collision of the Hikurangi Plateau and Chatham Rise with Hikurangi Trench and subduction of oceanic crust northeast of the North Island.

Hikurangi Plateau initially formed a part and now separated from the largest oceanic plateau on Earth, the Ontong Java Plateau, located in the southwestern Pacific Ocean (Neal *et al*. 1997). Hikurangi Margin and continental shelf of the North Island of the New Zealand

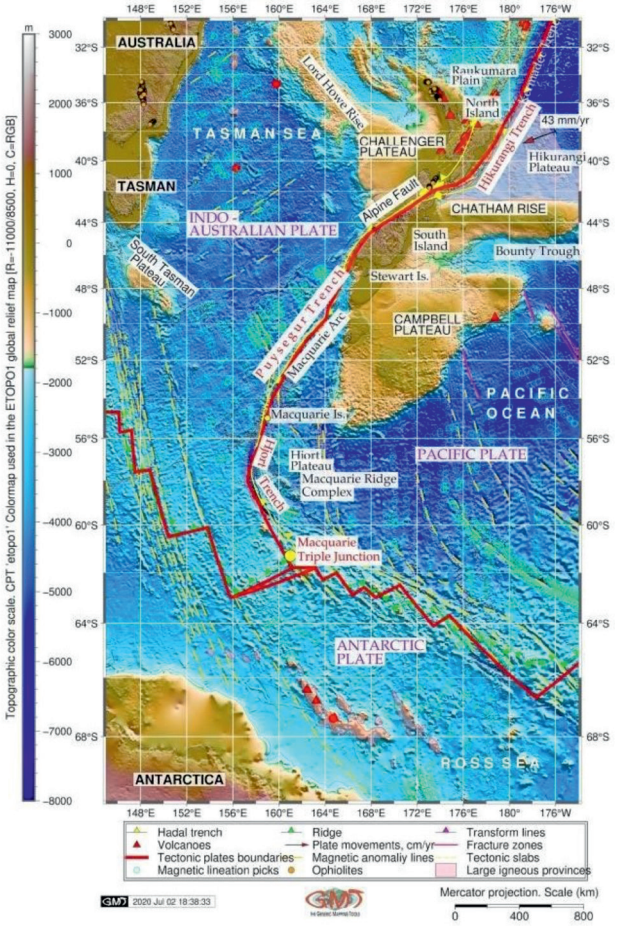

Fig. 2. Tectonic and geological settings of the study area, New Zealand region. The Pacific Plate subducts beneath the Indo-Australian Plate at the Hikurangi Trench; Indo- Australian Plate subducts beneath the Pacific Plate at the Puysegur and Hjort Trenches. Two subduction margins joined by dextral transform Alpine Fault, New Zealand (ed. by author)

Ryc. 2. Pozycja geotektoniczna badanego obszaru w regionie Nowej Zelandii. Płyta pacyficzna ulega subdukcji pod płytę indo-australijską wzdłuż rowu oceanicznego Hikurangi; w rowach oceanicznych Puysegur i Hjort subdukcja zachodzi w przeciwnym kierunku. Obydwie strefy subdukcji rozdziela prawoprzesuwczy uskok transformacyjny Alpine Fault, Nowa Zelandia (oprac. autorki)

is well studied through various geologic investigations, more specifically: bathymetric, hydro-acoustic investigations (Barnes *et al*. 2010), active tectonics. Palaeogeographic reconstruction of the evolution of topography/bathymetry in the region of Hikurangi (Jiao *et al*. 2015) uses advanced methods of the thermochronology. Further findings in exploration geology in the Hikurangi Trench with a special focus on methane seepage and gas hydrates in the underlying sediments are relatively well studied (e.g. Klaucke *et al*. 2010; Krabbenhoeft *et al*. 2010, 2013; Martin *et al*. 2010; Pecher *et al*. 2010; Wang *et al*. 2017) studies on subduction earthquakes in Holocene, coseismic coastal deformation and tsunamis (Berryman *et al*. 2011; Clark *et al*. 2019) which later on largely affected submarine geomorphology of the Hikurangi margin forming submerged terraces (Berryman 1993).

2.2. Puysegur Trench

Puysegur Trench has ca. 800 km in length, stretching from the most southern tip of the South Zone is associated with the Alpine Fault, which is the right-lateral transform fault boundary separating the Puysegur Trench and the northern Kermadec Trench (Beavan, Haines 2001). Macquarie Ridge Complex (MRC) is a dominantly translational structure accommodating right-lateral motion between the Australian and Pacific Plates and the Puysegur Trench, where Australian lithosphere subducts beneath the southwest corner of New Zealand on the Pacific Plate. The plate boundary south of New Zealand is located along the MRC which is crucial for understanding the tectonic structure of the region. Comparing to the Hikurangi, Puysegur/Hjort is younger (started at 16–8 Ma) and less developed (Sutherland *et al*. 2006). The Indo--Australian Plate subducts beneath the Puysegur Bank and the Fiordland Massif forming Puysegur Trench.

2.3. Hjort Trench

Hjort Trench continues Puysegur Trench southwards from the Macquarie Island and extends until the Macquarie Triple Junction. It presents a linear topographic depression south of Macquarie Island in the southwest Pacific Ocean (Fig. 2). Hjort Trench lies in an area of transpression where plate boundary transitions from a transform boundary to a convergent one. Hence, this region shows how a transform boundary with a vertical (near-vertical) transform fault becomes an area of under-thrusting (Meckel *et al*. 2003). The deepest point of Hjort Trench is ca. 6.3 km b.s.l. Eastwards, the Hjort ridge follows the general curve of the Hjort Trench, separating it from the Hjort Plateau.

Hjort Trench is characterized by an oblique subduction zone geoid anomaly. Large 1924 earthquake occurred in the northern Hjort Trench which suggest a thrust focal mechanism and active subduction of young oceanic lithosphere beneath older oceanic lithosphere (Cazenave, Ruff 1985). Frequent seismic events, most less than 20 km deep, characterize the transpression along this plate boundary (Lodolo, Coren 1994). The southern segment of the Alpine Fault on the South Island continues into the Tasman Sea Basin and finishes at the Puysegur Trench (Fig. 2). The oceanic Indo-Australian plate subducts eastwards through the Puysegur Trench under the Pacific Plate.

Geologic events during the tectonic historical records of this region, such as Eocene-Oligocene rifting as well as Miocene-Quaternary strike-slip, crustal thinning in the Solander Basin, development of the oblique subduction zone in the Puysegur Trench, are studied by processing seafloor relief data and interpretation of the seismic and bathymetric cross-section profiles acquired over the Puysegur Trench area (Lamarche *et al*. 1997; Melhuish *et al*. 1999; Lamarche, Lebrun 2000).

3. Methods

3.1. Topographic mapping

The area selected for the data set lies in the southern Pacific Ocean and includes three trenches: Puysegur, Hjort and Hikurangi off New Zealand coast. The region is characterized by a geologically complex history and current situation with oblique subduction zone and subduction scissors. Such complex bathymetry exhibits considerable geomorphological variability among three trenches: there are differences caused by seamounts and seafloor obstructing natural curvatures of the trenches.

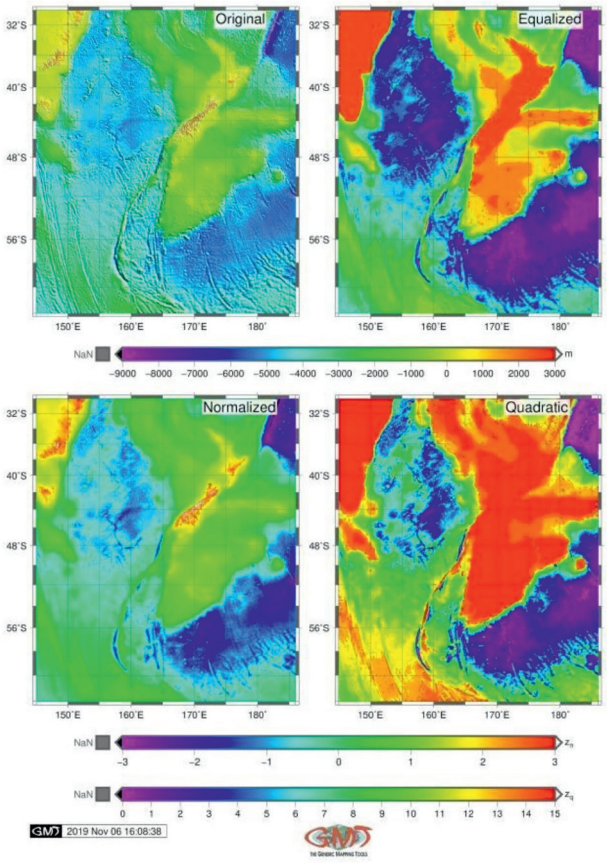

Fig. 3. Histogram equalization on the topography grids, ETOPO1 (ed. by author)

Ryc. 3. Wyrównanie histogramu na siatkach topograficznych, ETOPO1 (oprac. autorki)

High-resolution bathymetric data is important for mapping trench shape in a cross-section and to identify clearly its geomorphology. For these reasons, GEBCO bathymetric grid (GEBCO Compilation Group 2020) was selected for topographic mapping (Fig. 1). Pixel size at a course resolution bathymetric maps (ETOPO5) may reduce accuracy. Hence, ETOPO1 and GEBCO datasets were chosen. Among the two, the GEBCO grid was used as the base geodata source due to its high resolution: 15- arc second. The GEBCO (https://www.gebco.net/) grid uses as a base Version 1 of the SRTM15+ data set (Olson *et al*. 2014) which in turn is based on version 11 of SRTM30+ (Becker *et al*. 2009; Sandwell *et al*. 2014), updated by

gridded bathymetric data sets. The geoid and gravity (Fig. 4 and 5) are modeled based on the Earth Gravitational Model EGM96 dataset (Lemoine *et al*. 1998).

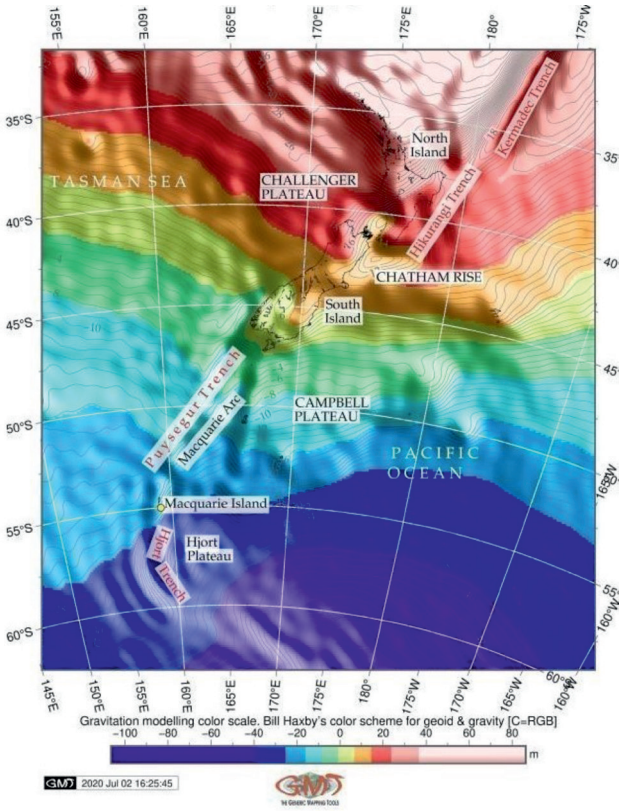

Fig. 4. Geoid model visualization based on the EGM96: New Zealand region, Hikurangi, Puysegur and Hjort Trenches (ed. by author)

Ryc. 4. Wizualizacja modelu geoidy na podstawie EGM96: region Nowej Zelandii, rowy oceaniczne Hikurangi, Puysegur i Hjort (oprac. autorki)

The quality of the two grids (GEBCO and ETOPO1) was compared and the data outputs assessed. Because the GEBCO grid has higher resolution than ETOPO1 (15 arc--second against 1 arc-minute, respectvely), ultimately the GEBCO was selected as the base map for modelling and visualization

The assessment of the ETOPO1 grid was included visualization of the four subplots of histogram equalization (Fig. 3). The smoothness of the grids intensities for ETOPO1 was improved by passing the output of ‚grdgradient' to ‚grdhisteq'. Comparative histogram equalization was performed by key GMT module ‚grdhisteq' to enhance visualization of the various ranges of the ETOPO1 grid (Fig. 3). Four subplots were generated to find values dividing grid files into equal area patches. The 'grdhisteq' module performs a histogram equalization of raster images. Using 'grdhisteq', the ASCII data values dividing the range of the initial raster data into cells segments was written to an output file. The '-C16' argument defines 16 cells. The resulting raster grid has an equal area in the images. Using 'makecpt' GMT module this output was then coloured according to the actual bathymetric values by following code: gmt makecpt - Crainbow -T- 9000/3000 > t.cpt. The explanations for the subplot with four maps (Fig. 3) is as follows:

Top left: The original map (top left) visualizes initial raster (artificial cpt 'rainbow') to highlight changes in elevation; Top right: equalized raster grid; Low left: normalized raster grid derived using -N argument that stands for Gaussian output, used to to receive data with smooth Gaussian distribution. The default standard normal scores were used for grid normalization. Low right: quadratic equalization plotted using following snippet: gmt grdhisteq hpt_relief.nc -Gout.nc -Q. Here, the '-Q' argument is output selecting quadratic histogram equalization, unlike the default linear one. The '-T-9000/3000' argument means range of the topographic elevations. The image was then visualized using ‚grdimage' module by code snippet: $gmt grdimage hpt_relief.nc -I+a45+nt1 -Ct.cpt - JM3i -Y6i -K -P -Bpxg5f5a10 -Bpyg4f2a8 -Bsxg5 - Bsyg4 -BWSne > ps.

In this code, the '-Ct.cpt' argument passes cpt created in the previous step for visualization; the ‚-JM3i' arguments explains the Mercator projection with 3 inches width; ‚- Y6i' argument plots the map with 6 inches distance from the previous one by Y axis; ‚-K' argument refers to the continuation of the code. The annotation was added using Unix 'echo' prog: echo $172 -33 Original" | gmt pstext - Rhpt_relief.nc -J-F+jBL+f12p -T -Gwhite@10 - Dj0.1i -O -K >> ps.

The 'grdhisteq' GMT module enables to write a raster grid with statistics based on cumulative distribution function. That means, after applying the 'grdhisteq' module, the output raster file has relative elevations in the same locations as the input file (that is, x, y). However, the values are modified to reflect their place in cumulative distribution with reference to the initial input file. This illustrates the principle of the equalization of the topographic grids by GMT module 'grdhisteq', as visualized on Fig. 3.

3.2. Digitizing cross-section profiles

Modelling and digitizing a series of the cross-section profiles along the trenches: Hikurangi, Puysegur and Hjort (Fig. 6 and 7) and plotting three graphs based on the retrieved tables (Fig. 8) was performed in GMT. Cross--section profiling is a technique used in geosciences to receive a sample of the selected segment in the study area and analyze variability of the studied elements along the track.

Automated methods have been explored in cartography, driven largely by the advantages of using machine-learning algorithms in cartographic routine, thus minimizing handmade routine, subjectivity in processes of the digitizing and vectorizing of the bathymetric data. Examples of such works is presented by Schenke, Lemenkova (2008); Lemenkova (2019e, 2019g, 2019h). GMT proposes more advanced solution in the automatization of the cross-sections through ML based digitizing that results in a series of the profile transects across the trench (Wessel, Smith 2018).

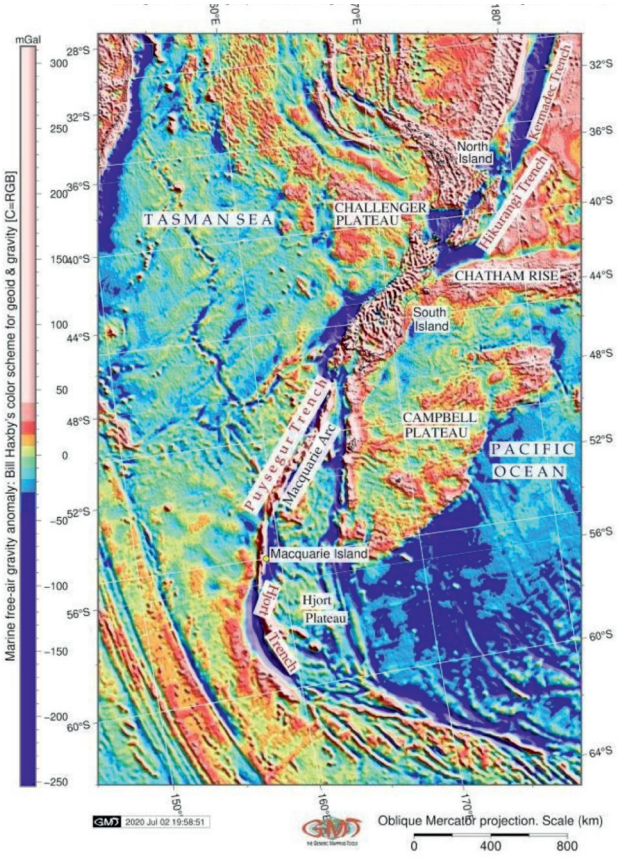

Fig. 5. Marine free-air gravity anomaly: Hikurangi, Puysegur and Hjort Trenches (ed. by author)

Ryc. 5. Morska anomalia grawitacyjna (redukcja wolnopowietrzna – Faye'a): rowy Hikurangi, Puysegur i Hjort (oprac. autorki)

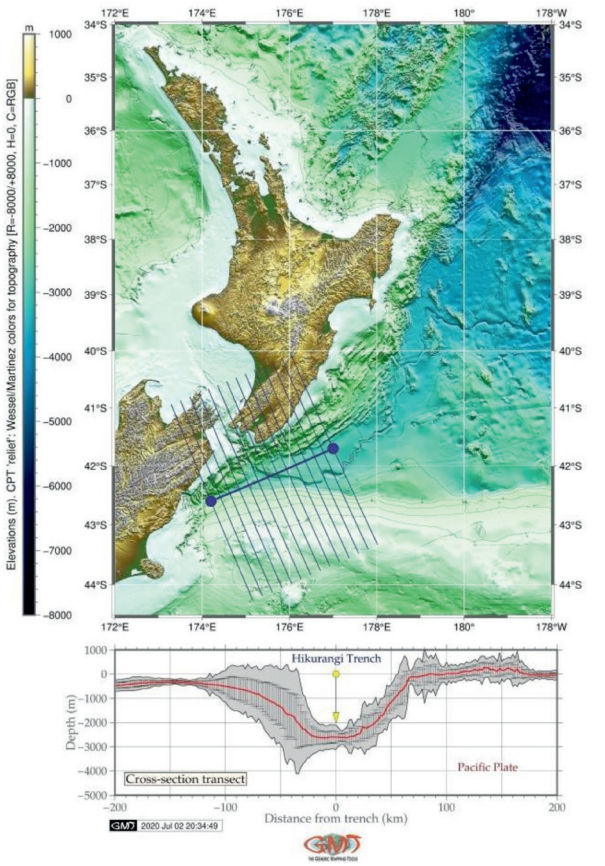

Fig. 6. Digitizing cross-section profiles in Hikurangi Trench, North Island (ed. by author)

Ryc. 6. Digitalizacja linii przekrojów w rowie Hikurangi, Wyspa Północna (oprac. autorki)

Two methods were tested in visualizing the profile: median and the mean (by GMT arguments '-Sm' for median and '-Sa' for mean). Of these two, median was selected as the best representing the empirical nature of the trench's shape. Although the 'mean' method shows fine interpolation, the 'median' approach shows the performance and visual representation of the trench within reasonable reflection of its geomorphology. On the contrary, mean values are notable for smoothing the splines rather as a mathematical functions which lesser reflects the geographic phenomena of the objects. The uncertainties of the actual geomorphology are expected to exceed the theoretical interpolation of the actual geomorphology represented on the graphs. The shape of the trenches is highlighted as median using '-Sm' argument, Fig. 6 and Fig. 8.

4. Results

Whilst it serves as a terrain variable in this study to examine the geomorphic landform, the variation of the geomorphic slopes were compared for the three trenches and following findings noted: Hikurangi Trench has a trough-like flat wide bottom, steeper gradient slope on the North Island flank (Fig. 6 and 8A).

Puysegur Trench (Fig. 8B: middle plot) has an asymmetric V-form with steep gradient on the eastern slopes and more gentle slope on the west. Hjort Trench has a symmetric shape form with comparative gradients on both western and eastern slopes (Fig. 8C, lower plot). The results of the comparison of the median values (red line on Figure 8 for three sub-plots) of three trenches show that selected segment of the Hikurangi Trench has shallower depths with maximal values approximately -2,600 m (Fig. 8A), while Puysegur Trench is reaching up to -6,000 m (Fig. 8B). The deepest values > 6,000 m for Hjort Trench (Fig. 8C). The surrounding relief of the Hjort Trench presents the most uneven terrain comparing to the other trenches. The neighboring terrain has a gentle slope on the oceanward side for Hikurangi Trench, and a steep slope on the eastern flank for Puysegur Trench, which is surrounded by more complex submarine relief along the Macquarie Arc (Fig. 2).

The statistical histograms for the transecting profiles of the Hikurangi, Puysegur and Hjort trenches are visualized on Figure 9. The evaluation of the descriptive statistics on bathymetry in three trenches and interpolation approaches shows following results. The shape of the histogram varies by the three trenches reflecting their geomorphology. Data distribution for the Hikurangi Trench

(Fig. 9B) demonstrates almost equal pattern for the depths from -600 m to -2,600 m with the samples observations not exceeding 60 for each sample bin (most data are detected at around 30 to 40 samples for a bin < 4%). Notable peak have data located on the shallow areas (shallower than -500 m) where maximal values are detected for the range -400 to -300 m (258 samples). We can clearly see a rising increase of data with depths below 500, that is a slope of the North Island (frequency 5% to 12%).

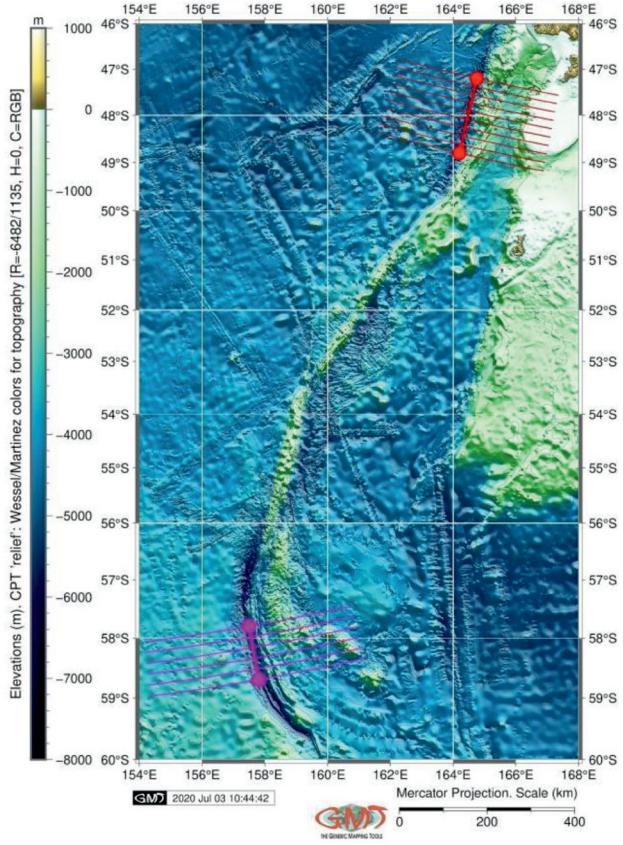

Fig. 7. Digitizing cross-section profiles in Puysegur and Hjort trenches, Macquarie Island Arc (ed. by author)

Ryc. 7. Digitalizacja linii przekrojów w rowach oceanicznych Puysegur i Hjort, łuk wyspowy Macquarie (oprac. autorki)

Puysegur Trench (Fig. 9A) has a bimodal type of data distribution with two peaks. The first peak has three notable bins range -4,250 to -4,500 m (373 samples detected, data frequency 18%), range -4,000 to 4,2 (182 samples, data frequency 9,6%) and -4,500 to -4,750 m (216 samples, data frequency 11,5%). The second peak covers depths from -2,750 to -3,000 m with the data frequency < 7,5%. The peak corresponds to the Macquarie Arc bordering the trench slope. Data distribution for the Hjort Trench (Fig. 9C) has a bell-shape form with a clear peak of data at depths -3,250 to -3,500 m (364 samples, 30% of data frequency). The abrupt decrease in the sample values off both flanks of the trench corresponds to the steep slope of the trench west off Hjort Plateau.

Spreading fabrics can be seen (Fig. 7) eastwards off the Puysegur Trench, together with minor ridges. This geomorphology is particularly well expressed along Macquarie Arc, between 51,5° and 54° where ridges might form due to the sedimentation processes. The ridges resembling elongated seamounts can be seen on the north-west side off the Puysegur Trench (Fig. 7) interspersed with minor troughs.

Geomorphic curvature and distribution of the seamounts near the Puysegur, Hjort and Hikurangi Trenches reflect the interplay between the complex tectonic processes occurring at a subducting tectonic plates and variations in the tension between the spreading ridges and the transform faults. In the northwest region off Puysegur Trench, GEBCO bathymetric data (Fig. 6 and 7) enable to see complex submarine relief: linearly expressed ridge geomorphology, a series of small elongated seamounts, minor troughs and flat seabed areas. The average depth of the seafloor deepens abruptly (Fig. 9A) from -4,750 (216 samples) to the -6,250 m (9 samples). The data distribution has a clear bimodal way for the Puysegur Trench with clear peaks at ranges -4,250 to -4,500 (373 samples) and at -2,750 to -3,000 m (140 samples). The histogram for the Hjort Trench (Fig. 9C) has a classic 'bell-shape' form with one peak in data distribution at range -3,250 to -3,500 m (364 samples).

The effect of using different histogram equalization algorithms was examined using subplots for data on ETOPO1 covering area for three trenches (Fig. 3). Equalization compression for bathymetry grids were tested as comparison for four grids: original, equalized, normalized, quadratic algorithms. The results for this step are demonstrated in Figure 3 showing a visual summary of a grid equalization by different GMT algorithms. Consistent cpt across all raster dataset grids where applied for better comparison.

From the analysis of histogram equalization algorithms it is notable that there are variations in the grids values obtained depending on the method: equalized, normalized, quadratic algorithms. This in itself means that the topic is worthy of further elaboration. Through the demonstrated example (Fig. 3) the effects of using different algorithms varying with raster dataset grids equalization can be notable. Cartographic functionality of the GMT is assessed by technical visualization of the produced maps, models and graphs as well as tested variety of map projections. In this study, following various cartographic projections were used for plotting maps: Mercator, Mollweide pseudo-cylindrical homolographic equal-area, Eckert IV equal-area pseudo-cylindrical, Lambert Azimuthal Equal-Area, Oblique Mercator.

5. Discussion

This study aimed to produce a set of the cross--section profiles for three deep-sea trenches varying in geomorphology which could be utilized at similar works for spatial marine data analysis and detailed seafloor mapping. The comparison of the geomorphology and

highlighted differences are presented for three trenches. In that sense the study objectives were achieved. GMT is aiming to enable cartographic visualization and modelling of a high standards, high-quality maps based on the raster/vector datasets which can be effectively used for mapping the shape of the seabed and submarine landforms, thereby providing the knowledge base to detail the topography of the World Ocean.

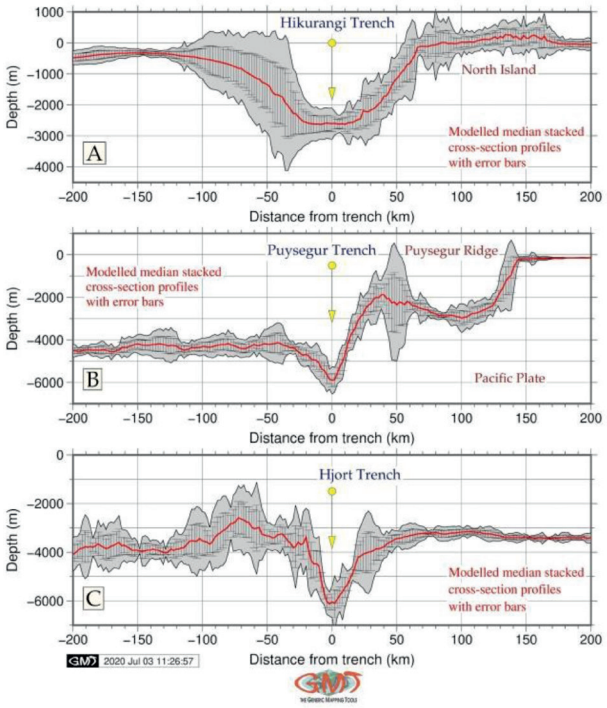

Fig. 8. Comparative analysis on geomorphic cross-sections by three trenches: Hikurangi, Puysegur and Hjort (ed. by author)

Ryc. 8. Analiza porównawcza profili batymetrycznych trzech rowów oceanicznych: Hikurangi, Puysegur i Hjort (oprac. autorki)

Approaches to the geological data analysis are diverse: ternary diagrams plotting (Reyes *et al*. 2010; Lemenkova 2019d), geophysical methods (Dahlin *et al*. 1999), swath--bathymetric mapping (Wells & Monahan 2002; Gauger *et al*. 2007; Nitsche *et al*. 2007), compression strength (Lindh 2004), various approaches to the data analysis, e.g. factor analysis, correlograms, cross-section plotting and visualization (Lemenkova 2018a, 2018b), geophysical and geomorphological modelling based on tectonic analysis and mapping (Serra *et al*. 2020; Gales *et al*. 2013; Lemenkova 2019c, 2019e). Apart from the statistical tools, a GIS data analysis is largely used in geological sciences. Comparing to the existing approaches based on various existing GIS software, e.g. ESRI ArcGIS (Suetova *et al*. 2005; Kuhn *et al*. 2006; Lemenkova 2011; Lemenkova *et al*. 2012; Klaučo *et al*. 2013a, 2013b, 2017), GMT is notable for its scripting based methodology. Plotting map in GMT evolves scripting and running a code from the console, unlike a GUI based GIS.

Modelling slope of the deep-sea trenches is important in relation to several reasons:

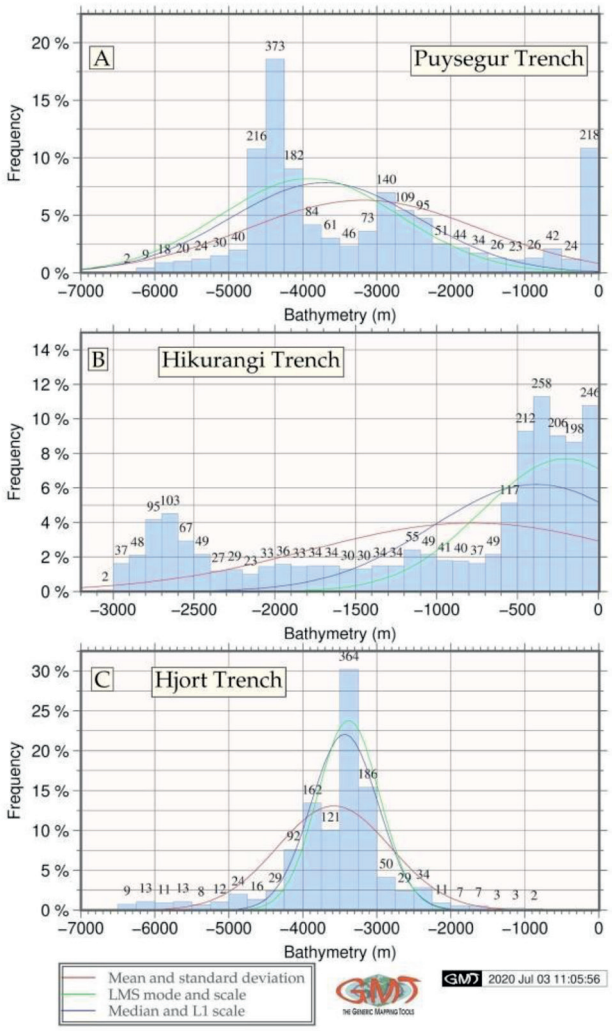

Fig. 9. Comparative analysis on data distribution by three trenches: Hikurangi, Puysegur and Hjort (ed. by author)

Ryc. 9. Analiza porównawcza rozkładu danych według trzech rowów: Hikurangi, Puysegur i Hjort (oprac. autorki)

1. Geomorphology of the trench presents a crucial characteristics for benthic habitat and hence serves as an environmental variable: more specifically, the stability of sediments which directly depend on the geomorphic slope characteristics, affects the ability of deep-sea fauna species to dwell on sediments.
2. Slope gradient is relevant as a geomorphological concept, since it impacts the stability of the geologic sediments and grain size.
3. Geomorphic slopes are factors inducing acceleration of ocean deep currents which is related to the environmental characteristics, such as ecological chain: food supply and exposure for the deep-sea fauna species.
4. Slope landforms and specific forms of the trench geomorphology induces erosion, movement, fall and replacements of sediments depending on their size.
5. Geomorphic characteristics of slopes eventually influence submarine landforms of the deep-sea trenches.

A phenomenon of the tectonic plates subduction explains the asymmetry of the deep-sea trenches. Subduction of one lithospheric plate to the Earth's mantle while another plate is being deformed induces a formation of the oceanic trench which eventually forms through filling the space between the plates. Necessarily, in case of the triple junction, the complexity of the bathymetric shape arises.

The depths of the Hikurangi, Puysegur and Hjort trenches are influenced by a variety of geologic processes and factors affecting their geomorphic shape and structure. Of these, the tectonic plates movements and slab geometry are the crucial factors controlling their form, gradient steepness and depths. This can be seen by the comparison of the visualized geophysical setting (Fig. 4 and 5) and geomorphology of the trench's seafloor (Fig. 6 and 7). Other factors include age and convergence rate of the plates, intermediate slab dip, width of sinking plate.

Generally, a strong correlation of the trench's axes with borders of the three lithospheric tectonic plates (Antarctic Plate, Pacific Plate and Info-Australian Plate) can be noted, which underpins strong correlation of the trench geomorphology with direction of the tectonic slab lineaments, as plate movements, geologic lineaments and extend of the fracture zones in the final end lead to the formation of the trench axis through the plates motions.

Local geologic settings, linear extension of the tectonic slabs, complex tectonic processes and sedimentation of the Hikurangi, Puysegur and Hjort trenches might explain variations in their geomorphic structure and shape of the submarine landforms, in particular, a zone of Macquarie Triple Junction in Southwest Pacific Ocean, Antarctic.

6. Conclusion

As the utility of the seafloor-mapping technology, a GMT scripting was demonstrated as a case study for comparative analysis of the three trenches, methods of visualization through GMT modules for thematic mapping of the topographic and geologic settings (Fig. 1 and 2), topographic statistical smoothing (Fig. 3) geoid and gravity fields (Fig. 4 and 5), cross-section profile digitizing (Fig. 6 and 7), geomorphic plotting (Fig. 8) and statistical visualization (Fig. 9).

Applying GMT techniques to seafloor mapping on Hikurangi, Puysegur and Hjort Trenches off New Zealand enabled to model geomorphology of the three trenches by tested methods (Lemenkova 2019f, 2020) and visualize corresponding geologic conditions; each trench was distinguished by specific geomorphic shape of the submarine landform, geologic substrate, complexity of the tectonic settings and historical development of the lithospheric plates movements in this area.

The data on bathymetry has been modeled through GMT based cross-section profiling for the three trenches, respectively, and compared. The maximal depths in the segments of the three trenches derived from digitized GEBCO grid were used for comparative analysis and visualized at histograms. Hikurangi Trench, which is also often referred as trough proved to have more trough-like shape form in its cross-section, while Puysegur and Hjort trenches have classic 'V'-form. Of all three trenches, Hjort Trench has the steepest slope gradient. The GMT demonstrated to be is a powerful cartographic toolset to visualize geological, geophysical and topographic maps, model geomorphic cross-sections and perform descriptive statistical analysis on the data retrieved from the automatic digitizing.

Cross-section modelling approach is based on the newly developed methods of the computed based data analysis and visualization of the transect x y z grids in topographical research (Harris *et al*. 2014; Hodgson *et al*. 2014; Bursztyn *et al*. 2015; Niyazi *et al*. 2018; Wessel, Smith 2018; Lemenkova 2019a, 2019b; Akan *et al*. 2020; Brothers *et al*. 2020; McCalpin *et al*. 2020; O'Brien *et al*. 2020; Trevisan *et al*. 2020), adapted to the geomorphic mapping as a basis for mapping submarine geomorphology. Automated cross-sectioning model is based on primarily the 'grdtrack' module and considers three principal variables: length of the transect segment, distance between the samples, density of sampling, which in this study were accepted as: track 400 km long, spaces 20 km along the selected segment of the trench, and density 2 km. These variables were selected for script and then have shaped the current cross-section shapes of the landforms and defined curvatures of the modeled transects as median with errors visualized in three trenches (Fig. 8). The X axis of the profiles (Fig. 8 A, B, C), reflects the perpendicular cross segment, the Y axis is modeled based on the bathymetry data and elevation characteristics by 'psxy' module. The graph is visualized based on the numerical model received through the digitizing of the cross-section profiles for each of the three trenches.

Three types of the deep-sea trench shapes have been then identified for the detailed seafloor mapping and further exploration. The open-source GMT approach represents a cost-effective approach to visualize seafloor in a geographically remotely located areas such as hadal trenches. The approach also delivers a knowledge base upon which more detailed studies on links between geology, tectonics and bathymetry can be identified and founded. Hikurangi Trench presented unique characteristics of the seafloor as trough-shaped form.

By recognizing the geomorphic shape and geologic environments at the seabed, distinctly different from Puysegur and Hjort Trenches, a gradual decrease of depths along the slope of the North Island was observed. Targeted seafloor mapping in cross-sections highlighted active seafloor processes have created unique geomorphic picture for the three trenches.

Acknowledgements

The author gratefully acknowledges the anonymous referees for their comments and review which improved the initial manuscript. The research was performed during the author's study in Ocean University of China and funded by China Scholarship Council (CSC), State Oceanic Administration (SOA), Marine Scholarship of China, Grant Nr. 2016SOA002, People's Republic of China, and implemented in the framework of the Project Nr. 0144-2019-0011, Schmidt Institute of Physics of the Earth, Russian Academy of Sciences.

7. References

Akan, Ç., McWilliams, J.C., Uchiyama, Y., 2020. Topographic and coastline influences on surf Eddies. Ocean Modelling 147, 101565. http://dx.doi.org/10.1016/j.ocemod.2019.101565

Amante, C., Eakins, B.W., 2009. Etopo1 1 arc-minute global relief model: Procedures, data sources and analysis. NOAA technical memorandum. http://dx.doi.org/10.7289/V5C8276M

Ballance, P.F., 1976. Evolution of the upper Cenozoic magmatic arc and plate boundary in northern New Zealand. Earth and Planetary Science Letters 28, 356–370. http://dx.doi.org/10.1016/0012-821X(76)90197-7

Barker, D.H.N., Sutherland, R., Henrys, S., Bannister, S., 2009. Geometry of the Hikurangi subduction thrust and upper plate, North Island, New Zealand. Geochemistry Geophysics Geosystems 10, 1–23. (Q02007). http://dx.doi.org/ 10.1029/2008GC002153

Barnes, P.M., Lamarche, G., Bialas, J., Henrys, S., Pecher, I., Netzeband, G.L., Crutchley, G., 2010. Tectonic and geological framework for gas hydrates and cold seeps on the Hikurangi subduction margin, New Zealand. Marine Geology 272, 26–48.

Barnes, P.M., Mercier de Lepinay, B., 1997. Rates and mechanics of rapid frontal accretion along the very obliquely convergent southern Hikurangi margin, New Zealand. Journal of Geophysical Research 102, 24931–24952. http://dx.doi.org/10.1029/97JB01384

Beavan, J., Haines, J., 2001. Contemporary horizontal velocity and strain rate fields of the Pacific-Australian plate boundary zone through New Zealand. Journal of Geophysical Research: Solid Earth 106, 741–770. http://dx.doi.org/10.1029/2000JB900302

Becker, J.J., Sandwell, D.T., Smith, W.H.F., Braud, J., Binder, B., Depner, J., Fabre, D., Factor, J., Ingalls, S., Kim, S.-H., Ladner, R., Marks, K., Nelson, S., Pharaoh, A., Trimmer, R., Von Rosenberg, J., Wallace, G., Weatherall, P., 2009. Global Bathymetry and Elevation Data at 30 Arc Seconds Resolution: SRTM30_PLUS. Marine Geodesy 32 (4), 355–371.

Berryman, K., Ota, Y., Miyauchi, T., Hull, A., Clark, K., Ishibashi, K., Litchfield, N., 2011. Holocene paleoseismic history of upper-plate faults in the Southern Hikurangi subduction margin, New Zealand, deduced from marine terrace records. Bulletin of the Seismological Society of America 101, 2064–2087.

Berryman, K.R., 1993. Distribution, age, and deformation of Late Pleistocene marine terraces at Mahia peninsula, Hikurangi subduction margin, New Zealand. Tectonics 12, 1365–1379. http://dx.doi.org/10.1029/93TC01543

Brothers, D.S., Miller, N.C., Barrie, J.V., Haeussler, P.J., Greene, H.G., Andrews, B.D., Zielke, O., Watt, J., Dartnell, P., 2020. Plate boundary localization, slip-rates and rupture segmentation of the Queen Charlotte Fault based on submarine tectonic geomorphology. Earth and Planetary Science Letters 530, 115882. http://dx.doi.org/10.1016/j.epsl.2019.115882

Bursztyn, N., Pederson, J.L., Tressler, C., Mackley, R.D., Mitchell, K.J., 2015. Rock strength along a fluvial transect of the Colorado Plateau – quantifying a fundamental control on geomorphology. Earth and Planetary Science Letters 429, 90–100. http://dx.doi.org/10.1016/j.epsl.2015.07.042

Cazenave, A., Ruff, L., 1985. Seasat geoid anomalies and the macquarie ridge complex. Food and agriculture organization of the united nations.

Clark, K., Howarth, J., Litchfield, N., Cochran, U., Turnbull, J., Dowling, L., Wolf, F., 2019. Geological evidence for past large earthquakes and tsunamis along the Hikurangi subduction margin, New Zealand. Marine Geology 412, 139–172.

Dahlin, T., Svensson, M., Lindh, P., 1999. DC Resistivity and SASW for Validation of Efficiency in Soil Stabilisation Prior to Road Construction. Procs. EEGS'99, Budapest, Hungary, 6–9 September 1999, Ls5, 1–3. http://dx.doi.org/10.3997/2214-4609.201406466

Gales, J.A., Larter, R.D., Mitchell, N.C., Dowdeswell, J.A., 2013. Geomorphic signature of Antarctic submarine gullies: Implications for continental slope processes. Marine Geology 337, 112–124. http://dx.doi.org/10.1016/j.margeo.2013.02.003

Gauger, S., Kuhn, G., Gohl, K., Feigl, T., Lemenkova, P., Hillenbrand, C., 2007. Swath-bathymetric mapping. Reports on Polar and Marine Research 557, 38–45.

GEBCO Compilation Group 2020. GEBCO 2020 Grid. http://dx.doi.org/10.5285/a29c5465-b138-234d-e053-6c86abc040b9

Greinert, J., Lewis, K.B., Bialas, J., Pecher, I.A., Rowden, A., Bowden, D.A., Linke, P., 2010. Methane seepage along the Hikurangi Margin, New Zealand: Overview of studies in 2006 and 2007 and new evidence from visual, bathymetric and hydroacoustic investigations. Marine Geology 272, 6–25.

Harris, P.T., Barrie, J.V., Conway, K.W., Greene, H.G., 2014. Hanging canyons of Haida Gwaii, British Columbia, Canada: Fault-control on submarine canyon geomorphology along active continental margins. Deep Sea Research Part II: Topical Studies in Oceanography 104, 83–92. http://dx.doi.org/10.1016/j.dsr2.2013.06.017

Hodgson, D.A., Graham, A.G.C., Griffiths, H.J., Roberts, S.J., Cofaigh, C.Ó., Bentley, M.J., Evans, D.J.A., 2014. Glacial history of sub-Antarctic South Georgia based on the submarine geomorphology of its fjords. Quaternary Science Reviews 89, 129–147. http://dx.doi.org/10.1016/j.quascirev.2013.12.005

Jiao, R., Seward, D., Little, T.A., Kohn, B.P., 2015. Unroofing of fore-arc ranges along the Hikurangi Margin, New Zealand: Constraints from low-temperature thermochronology. Tectonophysics 656, 39–51.

Klaucke, I., Weinrebe, W., Petersen, C.J., Bowden, D., 2010. Temporal variability of gas seeps offshore New Zealand: Multi-frequency geoacoustic imaging of the Wairarapa area, Hikurangi margin. Marine Geology 272, 49–58. http://dx.doi.org/10.1016/j.margeo.2009.02.009

Klaučo, M., Gregorova, B., Stankov, U., Markovic, V., Lemenkova, P., 2013a. Determination of ecological significance based on geo-statistical assessment: A case study from the Slovak Natura 2000 protected area. Central European Journal of Geosciences 5, 28–42.

Klaučo, M., Gregorová, B., Stankov, U., Marković, V., Lemenkova, P., 2013b. Interpretation of Landscape Values, Typology and Quality Using Methods of Spatial Metrics for Ecological Planning. 54th International Conference Environmental & Climate Technologies, October 14, 2013. Riga, Latvia.

Klaučo, M., Gregorová, B., Stankov, U., Marković, V., Lemenkova, P., 2017. Land planning as a support for sustainable development based on tourism: A case study of Slovak Rural Region. Environmental Engineering and Management Journal 2 (16), 449–458.

Krabbenhoeft, A., Bialas, J., Klaucke, I., Crutchley, G., Papenberg, C., Netzeband, G.L., 2013. Patterns of subsurface fluid-flow at cold seeps: The Hikurangi Margin, offshore New Zealand. Marine and Petroleum Geology 39, 59–73.

Krabbenhoeft, A., Netzeband, G.L., Bialas, J., Papenberg, C., 2010. Episodic methane concentrations at seep sites on the upper slope Opouawe Bank, southern Hikurangi Margin, New Zealand. Marine Geology 272, 71–78. http://dx.doi.org/10.1016/j.margeo.2009.08.001

Kuhn, G., Hass, C., Kober, M., Petitat, M., Feigl, T., Hillenbrand, C.D., Kruger, S., Forwick, M., Gauger, S., Lemenkova, P., 2006. The response of quaternary climatic cycles in the South-East Pacific: Development of the opal belt and dynamics behavior of the West Antarctic ice sheet. Expeditionsprogramm Nr. 75 ANT XXIII/4.

Lamarche, G., Collot, J.-Y., Wood, R.A., Sosson, M., Sutherland, R., Delteil, J., 1997. The Oligocene-Miocene Pacific-Australian plate boundary, South of New Zealand: Evolution from oceanic spreading to strike-slip faulting. Earth and Planetary Science Letters 148, 129–139.

Lamarche, G., Lebrun, J.-F., 2000. Transition from strike-slip faulting to oblique subduction: Active tectonics at the Puysegur Margin, South New Zealand. Tectonophysics 316, 67–89.

Lemenkova, P., 2011. Seagrass mapping and monitoring along the coasts of Crete, Greece. M.Sc. Thesis, University of Twente.

Lemenkova, P., Promper, C., Glade, T., 2012. Economic Assessment of Landslide Risk for the Waidhofen a.d. Ybbs Region, Alpine Foreland, Lower Austria, [In:] Eberhardt, E. *et al*. (eds.), Protecting society through improved understanding. 11th International Symposium on Landslides & the 2nd North American Symposium on Landslides & Engineered Slopes (NASL), June 2–8, 2012. Banff, AB, Canada, 279–285.

Lemenkova, P., 2018a. Factor Analysis by R Programming to Assess Variability Among Environmental Determinants of the Mariana Trench. Turkish Journal of Maritime and Marine Sciences 4, 146–155.

Lemenkova, P., 2018b. R scripting libraries for comparative analysis of the correlation methods to identify factors affecting Mariana Trench formation. Journal of Marine Technology and Environment 2, 35–42.

Lemenkova, P., 2019a. GMT Based Comparative Analysis and Geomorphological Mapping of the Kermadec and Tonga Trenches, Southwest Pacific Ocean. Geographia Technica 14, 39–48.

Lemenkova, P., 2019b. Topographic surface modelling using raster grid datasets by GMT: Example of the Kuril-Kamchatka Trench, Pacific Ocean. Reports on Geodesy and Geoinformatics 108, 9–22.

Lemenkova, P., 2019c. Geophysical Modelling of the Middle America Trench using GMT. Annals of Valahia University of Targoviste. Geographical Series 19 (2), 73–94.

Lemenkova, P., 2019d. Statistical Analysis of the Mariana Trench Geomorphology Using R Programming Language. Geodesy and Cartography 45, 57–84.

Lemenkova, P., 2019e. Testing Linear Regressions by StatsModel Library of Python for Oceanological Data Interpretation. Aquatic Sciences and Engineering 34, 51–60. http://dx.doi.org/10.26650/ASE2019547010

Lemenkova, P., 2019f. Geomorphological modelling and mapping of the Peru-Chile Trench by GMT. Polish Cartographical Review 51 (4), 181–194.

Lemenkova, P., 2019g. Automatic Data Processing for Visualising Yap and Palau Trenches by Generic Mapping Tools. Cartographic Letters 27 (2), 72–89.

Lemenkova, P., 2019h. AWK and GNU Octave Programming Languages Integrated with Generic Mapping Tools for Geomorphological Analysis. GeoScience Engineering 65 (4), 1–22.

Lemenkova, P., 2020. Variations in the bathymetry and bottom morphology of the Izu-Bonin Trench modelled by GMT. Bulletin of Geography. Physical Geography Series 18 (1), 41–60. http://dx.doi.org/10.2478/bgeo-2020-0004

Lemoine, F.G., Kenyon, S.C., Factor, J.K., Trimmer, R.G., Pavlis, N.K., Chinn, D.S., Cox, C.M., Klosko, S.M., Luthcke, S.B., Torrence, M.H., Wang, Y.M., Williamson, R.G., Pavlis, E.C., Rapp, R.H., Olson, T.R., 1998. NASA/TP-1998-206861: The Development of the Joint NASA GSFC and NIMA Geopotential Model EGM96, NASA Goddard Space Flight Center, Greenbelt, Maryland, 20771 USA.

Lindh, P., 2004. Compaction- and strength properties of stabilised and unstabilised fine-grained tills. Lund University. PhD Thesis.

Lodolo, E., Coren, F., 1994. The Westernmost Pacific Antarctic plate boundary in the vicinity of the Macquarie triple junction. Terra Antarctica 1, 158–161.

Martin, R.A., Nesbitt, E.A., Campbell, K.A., 2010. The effects of anaerobic methane oxidation on benthic foraminiferal assemblages and stable isotopes on the Hikurangi Margin of eastern New Zealand. Marine Geology 272, 270–284.

McCalpin, J.P., Gutierrez, F., Bruhn, R.L., Guerrero, J., Pavlis, T.L., Lucha, P., 2020. Tectonic geomorphology and late Quaternary deformation on the Ragged Mountain fault, Yakutat microplate, South Coastal Alaska. Geomorphology 351, 106875. http://dx.doi.org/10.1016/j.geomorph.2019.106875

Meckel, T.A., Coffin, M.F., Mosher, S., Symonds, P., Bernardel, G., Mann, P., 2003. Underthrusting at the Hjort Trench, Australian-Pacific plate boundary: Incipient subduction? Geochemistry, Geophysics, Geosystems 4, 1099. http://dx.doi.org/10.1029/2002GC000498

Melhuish, A., Sutherland, R., Davey, F.J., Lamarche, G., 1999. Crustal structure and neotectonics of the Puysegur oblique subduction zone, New Zealand. Tectonophysics 313, 335–362.

Neal, C.R., Mahoney, J.J., Kroenke, L.W., Duncan, R.A., Petterson, M.G., 1997. The Ontong Java Plateau. Geophysical Monograph Series 100, 183–216.

Nicol, A., Wallace, L.M., 2007. Temporal stability of deformation rates: Comparison of geological and geodetic observations, Hikurangi subduction margin, New Zealand. Earth and Planetary Science Letters 258, 397–413. http://dx.doi.org/10.1016/j.epsl.2007.03.039

Nitsche, F.O., Jacobs, S.S., Larter, R.D., Gohl, K., 2007. Bathymetry 393 of the Amundsen Sea continental shelf: Implications for geology, oceanography, and glaciology. Geochemistry, Geophysics, Geosystems, 395 8. http://dx.doi.org/10.1029/2007GC001694

Niyazi, Y., Eruteya, O.E., Omosanya, K.O., Harishidayat, D., Johansen, S.E., Waldmann, N., 2018. Seismic geomorphology of submarine channel-belt complexes in the Pliocene of the Levant Basin, offshore central Israel. Marine Geology 403, 123–138. http://dx.doi.org/10.1016/j.margeo.2018.05.007

O'Brien, P.E., Post, A.L., Edwards, S., Martin, T., Caburlotto, A., Donda, F., Leitchenkov, G., Romeo, R., Duffy, M., Evangelinos, D., Holder, L., Leventer, A., López-Quirós, A., Opdyke, B.N., Armand, L.K., 2020. Continental slope and rise geomorphology seaward of the Totten Glacier, T East Antarctica (112°E–122°E). Marine Geology 427, 106221.

Olson, C.J., Becker, J.J., Sandwell, D.T., 2014. A new global bathymetry map at 15 arcsecond resolution for resolving seafloor fabric: SRTM15_PLUS, AGU Fall Meeting Abstracts 2014.

Pecher, I.P., Henrys, S.A., Wood, W.T., Kukowski, N., Crutchley, G.J., Fohrmann, M., Faure, K., 2010. Focussed fluid flow on the Hikurangi Margin, New Zealand – Evidence from possible local upwarping of the base of gas hydrate stability. Marine Geology 272, 99–113. http://dx.doi.org/10.1016/j.margeo.2009.10.006

Pysklywec, R.N., Ellis, S.M., Gorman, A.R., 2010. Three-dimensional mantle lithosphere deformation at collisional plate boundaries: A subduction scissor across the South Island of New Zealand. Earth and Planetary Science Letters 289, 334–346.

Reyes, A.G., Christenson, B.W., Faure, K., 2010. Sources of solutes and heat in low-enthalpy mineral waters and their relation to tectonic setting, New Zealand. Journal of Volcanology and Geothermal Research 192, 117–141. http://dx.doi.org/10.1016/j.jvolgeores.2010.02.015

Reyners, M., 2013. The central role of the Hikurangi Plateau in the Cenozoic tectonics of New Zealand and the Southwest Pacific. Earth and Planetary Science Letters 361, 460–468.

Reyners, M., Eberhart-Phillips, D., Bannister, S., 2011. Tracking repeated subduction of the Hikurangi Plateau beneath New Zealand. Earth and Planetary Science Letters 311, 165–171.

Sandwell, D.T., Müller, R.D., Smith, W.H.F., Garcia, E., Francis, R., 2014. New global marine gravity model from CryoSat-2 and Jason-1 reveals buried tectonic structure. Science, 346, 6205, 65–67. http://dx.doi.org/10.1126/science.1258213

Schenke, H.W., Lemenkova, P., 2008. Zur Frage der Meeresboden--Kartographie: Die Nutzung von AutoTrace Digitizer für die Vektorisierung der Bathymetrischen Daten in der Petschora-See. Hydrographische Nachrichten 81, 16–21.

Serra, C.S., Martínez-Loriente, S., Gràcia, E., Urgeles, R., Vizcaino, A., Perea, H., Bartolome, R., Pallàs, R., Lo Iacono, C., Diez, S., Dañobeitia, J., Terrinha, P., Zitellini, N. 2020. Tectonic evolution, geomorphology and influence of bottom currents along a large submarine canyon system: The São Vicente Canyon (SW Iberian margin). Marine Geology 426, 106219. http://dx.doi.org/10.1016/j.margeo.2020.106219

Suetova, I., Ushakova, L., Lemenkova, P., 2005. Geoinformation mapping of the Barents and Pechora Seas. Geography and Natural Resources 4, 138–142.

Sutherland, R., Barnes, P., Uruski, C., 2006. Miocene-recent deformation, surface elevation, and volcanic intrusion of the overriding plate during subduction initiation, offshore southern Fiordland, Puysegur Margin, Southwest New Zealand. New Zealand Journal of Geology and Geophysics 49, 131–149.

Trevisan, A., Venema, V., Kollet, S., Rahman, M., 2020. The topographic control on land surface energy fluxes: A statistical approach to bias correction. Journal of Hydrology 584, 124669. http://dx.doi.org/10.1016/j.jhydrol.2020.124669

Wallace, L., Reyners, M., Cochran, U., Bannister, S., Barnes, P., Berryman, K., Power, W.L., 2009. Characterizing the seismogenic zone of a major plate boundary subduction thrust: The Hikurangi Margin. Geochemistry. Geophysics. Geosystems 10.

Wang, H., Crutchley, G.J., Stern, T., 2017. Gas hydrate formation in compressional, extensional and un-faulted structural settings – Examples from New Zealand's Hikurangi margin. Marine and Petroleum Geology 88, 69–80.

Wells, D., Monahan, D., 2002. IHO S44 Standards for Hydrographic surveys and the variety of requirements for bathymetric data. The Hydrographic Journal, 104, 9–16

Wessel, P., Smith, W.H.F., 2018. The Generic Mapping Tools. Version 4.5.18 Technical Reference and Cookbook. Computer software manual. U.S.A.